Light deflection and modulation through dynamic evolution of photoinduced waveguides

Germano Montemezzani, Mohammed Gorram, Nicolas Fressengeas, Flurin Juvalta, Mojca Jazbinsek, Peter Gunter

Light deflection and modulation through dynamic evolution of photoinduced waveguides

Germano Montemezzani,[1] **Mohamed Gorram,**[1] **Nicolas Fressengeas,**[1] **Flurin Juvalta,**[2] **Mojca Jazbinsek**[2] **and Peter Günter**[2]

[1] *Laboratoire Matériaux Optiques, Photonique et Systèmes (LMOPS) University Paul Verlaine – Metz and Supelec, CNRS UMR 7132, 2 rue E. Belin, F-57070 Metz, France*

[2] *Nonlinear Optics Laboratory, ETH Zurich, CH-8093 Zurich, Switzerland*

germano.montemezzani@metz.supelec.fr

Abstract: Light induced waveguides produced by lateral illumination of a photorefractive crystal show a complex dynamic evolution upon removal of the sustaining applied electric field. Using this effect, deflection and modulation of the guided light is realized by taking advantage of the screening and counter-screening of the space charge distribution. The spot separation upon deflection can exceed 10 times the original waveguide width. Numerical simulations of the refractive index evolution and beam propagation show a good agreement with the observations.

OCIS codes: (130.2790) Guided waves; (190.4390) Nonlinear optics, integrated optics; (190.5330) Photorefractive optics; (250.7360) Waveguide modulators.

References and links

1. Ph. Dittrich, G. Montemezzani, P. Bernasconi, and P. Günter, "Fast, reconfigurable light-induced waveguides," Opt. Lett. **24**, 1508–1510 (1999).
2. F. Juvalta, B. Koziarska-Glinka, M. Jazbinsek, G. Montemezzani, K. Kitamura and P. Günter, "Deep UV light induced, fast reconfigurable and fixed waveguides in Mg doped $LiTaO_3$," Opt. Express **14**, 8278–8289 (2006), http://www.opticsexpress.org/abstract.cfm?URI=oe-14-18-8278.
3. P. Zhang, D. Yang, J. Zhao and M. Wang, "Photo-written waveguides in iron-doped lithium niobate crystal employing binary optical masks," Opt. Eng. **45**, 074603 (2006).
4. M. F. Shih, M. Segev, G. Salamo, "Circular waveguides induced by two-dimensional bright steady-state photorefractive spatial screening solitons," Opt. Lett. **21**, 931–933 (1996).
5. G. Roosen and G.T. Sincerbox, "Optically generated light beam deflection," J. Appl.Phys. **54**, 1628–1630 (1983).
6. E. Voit, C. Zaldo and P. Günter, "Optically induced variable light deflection by anisotropic Bragg diffraction in photorefractive $KNbO_3$," Opt. Lett. **11**, 309–311 (1986).
7. B. Fischer and S. Sternklar, "Self Bragg matched beam steering using the double color pumped photorefractive oscillator," Appl. Phys. Lett. **51**, 74–75 (1987).
8. M.P. Petrov, A.P. Paugurt, V.V. Bryskin, S. Wevering, B. Andreas and E. Krätzig, "Dynamic light beam deflection caused by space charge waves in photorefractive crystals," Appl. Phys. B **69**, 341–344 (1999).
9. S. Honma, A. Okamoto and Y. Takayama, "Photorefractive duplex two-wave mixing and all-optical deflection switch," J. Opt. Soc. Am. B **18**, 974–975 (2001).
10. D. Kip, M. Wesner, E. Krätzig, V. Shandarov and P. Moretti, "All-optical beam deflection and switching in strontium-barium-niobate waveguides," Appl. Phys. Lett. **72**, 1960–1962 (1998).
11. W.L. She, Z.X. Yu and W.K. Lee, "Laser beam deflection in a photorefractive crystal induced by lateral beam movement," Opt. Commun. **135**, 342–346 (1997).
12. R. Mosimann, D. Haertle, M. Jazbinsek, G. Montemezzani and P. Günter, "Determination of the absorption constant in the interband region by photocurrent measurements," Appl. Phys. B **83**, 115-119 (2006).

13. K. Okamoto, *Fundamentals of optical waveguides* (Academic Press, San Diego, 2000).
14. G. P. Agrawal, *Nonlinear fiber optics*, 4th Ed., (Academic Press, Boston, 2007).
15. A. A. Zozulya and D. Z. Anderson, "Nonstationary self-focusing in photorefractive media," Opt. Lett. **20**, 837–839 (1995).
16. R. Ryf, M. Wiki, G. Montemezzani, P. Günter and A. A. Zozulya, "Launching one-transverse-dimension photorefractive solitons in $KNbO_3$ crystals," Opt. Commun. **159**, 339-348 (1999).
17. M. Klotz, H. Meng, G. J. Salamo, M. Segev and S. R. Montgomery, "Fixing the photorefractive soliton," Opt. Lett. **24**, 77–79 (1999).
18. I. Biaggio, "Recording speed and determination of basic materials properties," in: *Photorefractive Materials and Their Applications 2: Materials*, P. Günter and J. P. Huignard, eds., (Springer, New York, 2006), pp. 51-81.
19. N. Fressengeas, J. Maufoy and G. Kugel, "Temporal behavior of bidimensional photorefractive bright spatial solitons," Phys. Rev. E **54**, 6866-6875 (1996).
20. S. Ducharme, J. Feinberg and R. R. Neurgaonkar, "Electrooptic and piezoelectric measurements in photorefractive barium titanate and strontium barium niobate," IEEE J. Quantum Electron. **QE-23**, 2116-2121 (1987).
21. G. Montemezzani, P. Rogin, M. Zgonik and P. Günter, "Interband photorefractive effects: Theory and experiments in $KNbO_3$," Phys. Rev. B **49**, 2484–2502 (1994).
22. F. Juvalta, M. Jazbinsek, P. Günter and K. Kitamura, "Electro-optical properties of near-stoichiometric and congruent lithium tantalate at ultraviolet wavelengths," J. Opt. Soc. Am. B **23**, 276–281 (2006).

1. Introduction

Waveguides can be induced dynamically in a photoconductive electro-optic material by lateral illumination of the sample surface with a properly shaped control illumination in association with an applied electric field [1, 2], or, in alternative, by taking advantage of the photogalvanic response of the sample [3]. In the former case, the charge redistribution induced by the control illumination leads to the screening of the applied field, which can result in a locally increased refractive index in the illuminated region. The physical mechanism is similar to the one at work for waveguide formation by longitudinally propagating photorefractive bright spatial soliton beams [4]. Past investigations have shown that the steady-state shape of the waveguide reflects essentially the one of the light laterally illuminating the crystal. This is true in the case where the homogeneous conductivity of the crystal approaches the photoconductivity produced by the lateral control light. If this is not true, the waveguide shape can dynamically broaden beyond the width associated with the illumination. This situation is typically found in the absence of a homogeneous background radiation in low-conductivity materials. An example is $LiTaO_3$, for which an interesting waveguide-splitting phenomenon was recently discovered [2]. After the broadening of the waveguide, the removal of the applied field leads to the splitting of the guided light into two lobes outside the area originally occupied by the primary guide. This effect was qualitative explaned in terms of a re-screening of a space-charge distribution created by the initial screening of the applied field (double screening) [2].

One of the most attractive features of the photorefractive nonlinearity is the possibility for optical steering or modulation of a light beam. Light deflection and modulation via the photorefractive effect has been demonstrated in the past by different techniques, most of which rely on dynamic holography [5, 6, 7, 8, 9]. Variable light deflection was obtained by isotropic [5] or anisotropic diffraction [6] at a photorefractive Bragg grating tuned by a change of the recording wavelength. In alternative, a self Bragg matched configuration based on a double color pumped oscillator was also demonstrated [7]. Deflection of the reflected light was observed in sillenite crystals as a result of space-charge waves [8]. A photorefractive all-optical deflection switch was proposed in Ref. [9] by simultaneous interference of two pairs of waves and control of their relative phases (duplex two-wave mixing). Non-holographic beam deflection was demonstrated in He^+-implanted strontium barium niobate planar waveguides through the influence of a self-focused pump beam on a weaker probe beam [10]. In this case the effect was attributed to a combination of thermal and photorefractive effect. The lateral motion at constant velocity of a self-focused beam across a photorefractive crystal was also shown to give rise to strong

beam deflection as a result of the inertia of the refractive index change dynamics [11].

In this work we study the above mentioned waveguide splitting process in detail using the two low conductivity photorefractive crystals $Sr_xBa_{1-x}Nb_2O_6$ (SBN) and $LiTaO_3$. Upon removal of the electric field used to sustain the generation of the dynamic photoinduced waveguide, the light originally propagating in the waveguide is expelled from this region. We show that the double screening phenomenon mentioned above leads to a novel type of dynamic light deflection that may be controlled by adjusting different parameters. Among these the homogeneous background conductivity and the value of the electric field used during the waveguide recording step are the most important. Together with the shape of the lateral illumination, the background conductivity defines the initial conditions for the splitting process (the initial refractive index profile). The applied field controls the refractive index contrast and, together with the photorefractive response time, has a direct influence on the speed at which the light ”expulsion” takes place. The experimental observations are qualitatively confirmed by numerical simulations of the beam propagation based on a simplified model for the dynamic evolution of the refractive index distribution. This model can explain the exceptionally large light ”expulsion” distance observed in SBN. For this crystal the waveguide recording light is only weakly absorbed and the light reflected from the back surface of the crystal contributes in the definition of the shape of the refractive index distribution. Finally, it is shown that, using a periodically modulated applied electric field, a periodic switching of the output positions of the guided beam can be obtained under constant optical illumination. This new deflection-type switching is electrically controlled and requires the shaped control light merely as a kind of catalyst.

2. Experimental technique

Light induced waveguides were formed using a set-up similar to the one given in Ref. [2] except for the absence of the homogeneous background illumination. Fig. 1 gives a simplified scheme of the set-up. The control illumination defines the region and shape of the primary waveguide through the combination of the mask and the imaging optics. The probe wave guided in this guide is observed by the CCD camera at the output face of the crystal. The experiments

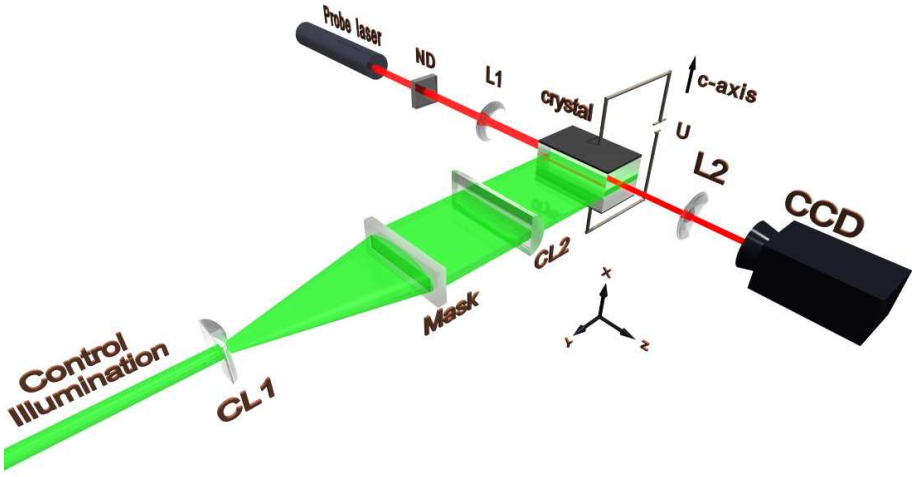

Fig. 1. Simplified scheme of the experimental set-up. L1, L2: spherical lenses; CL1, CL2: cylindrical lenses; ND: neutral density filter. A voltage U is applied to the photorefractive crystal.

presented in this work were performed with the electro-optic crystal strontium barium niobate ($Sr_xBa_{1-x}Nb_2O_6$, x=0.61) weakly doped with 0.02 mol% Ce, and, for comparison, with near stoichiometric $LiTaO_3$ with a Mg doping of 0.7 mol%. The dimensions of the crystals were $a \times b \times c = 10 \times 5 \times 5\,\mathrm{mm}^3$ and $a \times b \times c = 10 \times 4 \times 3\,\mathrm{mm}^3$, for SBN and $LiTaO_3$, respectively. The controlling light defining the waveguide shape was produced by transmission through a straight slit imaged onto the crystal and was at the wavelength $\lambda = 514$ nm for SBN and at $\lambda = 257$ nm for $LiTaO_3$. The former wavelength is moderately absorbed in SBN (with absorption constant $\alpha = 0.26\,\mathrm{cm}^{-1}$), while the latter is strongly absorbed in $LiTaO_3$ ($\alpha \approx 690\,\mathrm{cm}^{-1}$ [12]). An electric field was applied for both materials along the *c*-axis of the crystal in order to induce the waveguides in combination with the lateral control illumination. The direction of the field was such as to reduce the refractive index, what is generally known as the focusing case. The probe light was in both cases at $\lambda = 633$ nm and was polarized parallel to the crystal *c*-axis. Its propagation direction was along the longest direction for both crystals and its intensity was low, such that this wave was not influencing the waveguide formation. We concentrate in this work exclusively on the behavior observed upon removal or modulation of the electric field after a light induced waveguide was already formed by the process described in Refs. [1, 2] and reached steady-state. The applied electric field is therefore the only quantity that is varied during our measurements, i.e., we kept constant illumination conditions of the controlling light and constant coupling conditions for the red probe wave.

3. Beam splitting and deflection upon field removal

Figure 2 shows an example of the observed dynamics of the guided light exiting the SBN nonlinear crystal (back surface of the crystal imaged to a CCD camera). After the applied electric field is removed at the beginning of the movie the light splits into two lobes. The corresponding deflection angle varies with time and reaches a maximum before relaxing towards the center. In its final stage, after the end of the movie, the condition for natural diffraction is reached (absence of a waveguide). In this particular case the width of the one-dimensionally-guided wave before removal of the electric field was 16 μm (full-width at half maximum (FWHM) at the output crystal surface).

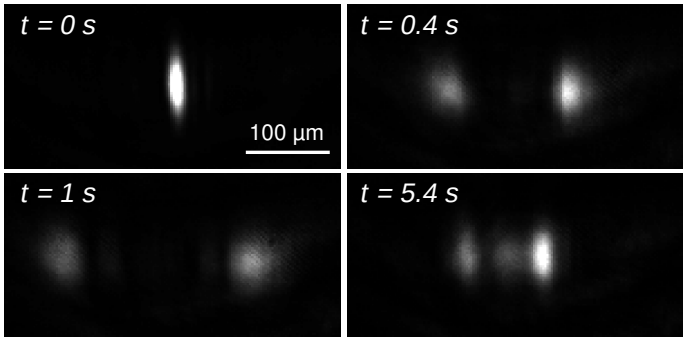

Fig. 2. (1.2 MB) Waveguide splitting and relaxation upon removal of the applied electric field ($E_0 = 4$ kV/cm) in the SBN crystal. The initial photoinduced waveguide was recorded to steady state using 514 nm light. The local intensity was 125 mW/cm^2 in the 25 μm wide imaged slit on the crystal lateral surface. The lateral illumination is maintained after removal of the applied field. The movie is in real time, the width of the imaged area is 410 μm.

Figure 3 shows the position of the "center of mass" of the two lobes as a function of time. All measurements were taken after a waveguide was recorded during the same time and at

the same intensity of the controlling light. The only difference between the three curves is the value of the electric field E_0 applied during waveguide recording. The initial fast displacement speed becomes gradually slower before inverting its direction; the system relaxes then towards the conditions were no waveguides longer exist. The maximum beam displacement is larger when the field E_0 was larger. In the case of SBN shown here, the total maximum separation be-

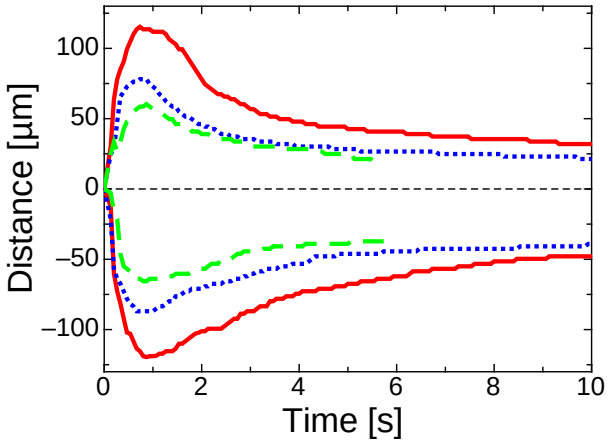

Fig. 3. Position of the "center of mass" of the expelled light lobes as a function of time. The initial photoinduced waveguides were recorded in SBN during 10 seconds to steady-state. The local intensity was 375 mW/cm^2 in the 25 μm wide imaged slit. The curves differ by the field E_0 applied during waveguide recording and removed at time $t = 0$. Red solid line: E_0= 4 kV/cm, blue dotted line: E_0= 2.4 kV/cm, green dashed line: E_0= 1.6 kV/cm.

tween the two lobes is about 235 μm for a field of $E_0 = 4$ kV/cm. Note that this displacement largely exceeds the width of the original projected waveguide (25 μm), as well as the width of the naturally diffracting probe wave at the output of the crystal in absence of a waveguide (FWHM$\approx$ 57 μm). Similar experiments performed in $LiTaO_3$ give generally smaller displacements of the light spots. As an example, Fig. 4 shows the near field image of the output surface of the $LiTaO_3$ crystal for the moment of maximum lobe distance. At the brighter spot position the separation is ≈ 92 μm, which is only slightly wider than the width of the naturally diffracted probe beam. It can be noticed that in this case the observed spots are slightly oblique. The spot distance increases to ≈ 105 μm closer to the surface illuminated by the UV control light and diminishes to ≈ 77 μm by moving down by about 70 μm. The reason for the appearance of these oblique spots will be discussed later.

We observe the exceptionally large light "expulsion" distance in SBN even though the guided light is still relatively well confined at the moment where the field is removed (see Fig. 2). This is different than the situation generally encountered in $LiTaO_3$, where, in absence of a background illumination, the probe light is no longer well guided at steady-state prior to field removal [2]. A more complex refractive index structure seems therefore to be responsible for our observations in SBN. We will discuss these aspects in detail in the next section.

4. Modeling of beam propagation upon field removal

4.1. SBN

In order to elucidate better the above anomalous waveguide splitting behavior, we have performed numerical simulations of the probe beam propagation by the beam propagation method

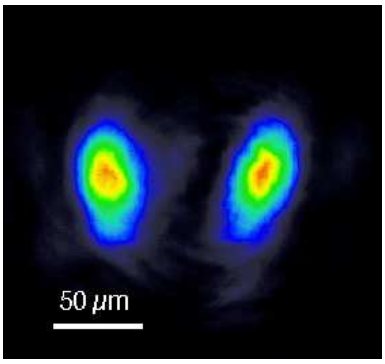

Fig. 4. Snapshot of waveguide splitting observed at the output surface of a $LiTaO_3$ crystal for the moment of maximum lobe separation. The electric field applied during recording of the primary waveguide was 5.5 kV/cm and the primary waveguide width was 20 μm. The UV control illumination comes from the top.

[13, 14]. In our model the one-dimensional refractive index profile is assumed to be invariant along the propagation direction z, but varies in time. Just after the removal of the electric field, the refractive index profile is assumed to possess the distribution

$$\Delta n(x) = \Delta n_0 \frac{I(x)}{I(x) + I_D}, \tag{1}$$

which applies to the case where the conventional photorefractive effect is at work. Here Δn_0 is the refractive index change amplitude proportional to the applied electric field according to $\Delta n_0 = n^3 r E_0/2$, where n is the average refractive index, r is the active effective electro-optic coefficient and E_0 is the field applied during waveguide recording. The quantity $I(x)$ is the spatially dependent intensity of the control light generating the waveguide. I_D is the dark intensity [15], that is the equivalent intensity producing the same density of mobile carriers than the one giving rise to the homogeneous component (average) conductivity of the crystal. Note that the dark intensity can be related to a combination of the dark conductivity and the photoconductivity due to a homogeneous background irradiation of the crystal, if the latter exists (see Ref. [16] for a detailed discussion). In the following the quantities $I(x)$ and I_D will be normalized in such a way that $I = 1$ corresponds to the intensity of the controlling light on the crystal in the center of a perfectly imaged slit. Expression (1) corresponds to the refractive index distribution due to steady-state screening of the applied field after formation of the primary waveguide, shifted up by the value Δn_0 as a result of the removal of the field E_0.

It was shown earlier, that a sufficiently high internal space-charge field opposite to the spontaneous polarization can induce ferroelectric domain reversal leading to the fixing of spatial soliton waveguides in SBN:75 crystals [17]. In our SBN:61 crystal, this kind of waveguide fixing was not observed for the range of parameters and for the experimental procedure used in our investigations. Therefore we can safely neglect the effect of domain reversal in the description of the dynamic evolution of our photoinduced waveguides. In this framework, the relaxation of the refractive index distribution upon removal of the applied electric field can be represented in the simplest approximation as

$$\Delta n(x,t) = \Delta n_0 \frac{I(x)}{I(x) + I_D} \exp\left[-t\,(I(x) + I_D)\right]. \tag{2}$$

Here the dimensionless time t has been normalized to the value of the photorefractive response time τ_{PR} for a normalized intensity equal to 1; τ_{PR} depends principally on the conductivity

and on the dielectric properties of the crystal [18]. The physical model underlying Eqs. (1) and (2) completely neglects all charge carrier diffusion effects. It assumes a fully local response dynamics, for which the local relaxation time is inversely proportional to the local total intensity [19]. Despite for the simplifying assumptions, this model maintains the most essential physical features and, as seen below, has the merit to reproduce the experimental observations in a satisfactory way.

A crucial aspect for the implementation of the model calculations is the choice of the light intensity distribution $I(x)$. In a first step we have performed several simulations by associating $I(x)$ solely with the control illumination directly incident on the region of the photoinduced waveguide (the green light propagating from bottom-left to top-right in Fig. 1). In the case of SBN we were never able to reproduce the observed behavior sufficiently well using a physically sound set of parameters. It appears therefore evident that the directly incident wave alone cannot lead to the strong repulsion observed. Our choice is therefore to consider an incoherent superposition of two components, $I(x) = I_1(x) + I_2(x)$. The first, $I_1(x)$, is the control light directly incident from outside. This is the wave discussed above that is intended to produce the narrow primary waveguide. We take the simplifying assumption that the slit defining the waveguide is perfectly imaged at some plane inside the crystal and that the waveguide is being probed very close to this plane, in the Fresnel diffraction regime of the imaged slit. The normalized intensity $I_1(x)$ can then be expressed as

$$I_1(x) = \frac{1}{2}\left([C(X_2) - C(X_1)]^2 + [S(X_2) - S(X_1)]^2 \right), \tag{3}$$

where $C(X)$ and $S(X)$ are the Fresnel cosine and sine integrals, respectively. The integration limits are $X_2 = \sqrt{2/(\lambda' d_1)}(x+a)$ and $X_1 = \sqrt{2/(\lambda' d_1)}(x-a)$, where $2a$ is the width of the imaged slit on the crystal, $\lambda' = \lambda/n$ is the light wavelength in the medium, and d_1 is the distance between the waveguide probing depth and the depth of ideal imaging. The second component, $I_2(x)$, consists of the same light after propagating inside the crystal to the other lateral surface and being reflected back towards the region of the waveguide. In most cases this reflected light is already in the Fraunhofer diffraction regime. The normalized intensity $I_2(x)$ can be calculated as well using Eq. (3), by replacing the distance d_1 with the total path distance d_2 from the ideal plane of perfect imaging to the back lateral surface, and back to the waveguide. In addition, the intensity $I_2(x)$ of the back reflected light has to be further normalized by a factor

$$K = \left(\frac{1-n}{1+n}\right)^2 \exp(-\alpha d_2), \tag{4}$$

that takes into account the Fresnel reflection and absorption of the controlling light (absorption constant = α). The light distribution $I(x) = I_1(x) + I_2(x)$ is depicted in Fig. 5(a) for a set of parameters proper to our crystal sample and experiments. The corresponding initial refractive index distributions according to Eq. (1) are shown in the same figure for three values of the normalized dark intensity I_D. The value $I_D = 0.005$ is consistent with the observed ratio between the formation time and the dark lifetime of the photoinduced structures in our crystal. The refractive index distribution of Fig. 5(b) shows that in this case the initial primary waveguide sits on a wider plateau of increased refractive index induced by the back reflected control light. As seen below, the refractive index contrast between the central primary guide and the plateau is nevertheless sufficient to guide the probe wave. For larger values of I_D (blue dotted line in Fig. 5(b)) one obtains a stronger and better confined initial central waveguide. In fact, if I_D exceeds the intensity level of the back reflected control light (which is about 3% at its maximum in our case), the plateau can be allmost completely eliminated. This is the concept used earlier for recording photoinduced waveguides with background illumination [1, 2], which experimentally leads to a much less dramatic dynamics upon field removal. On the other hand, for small

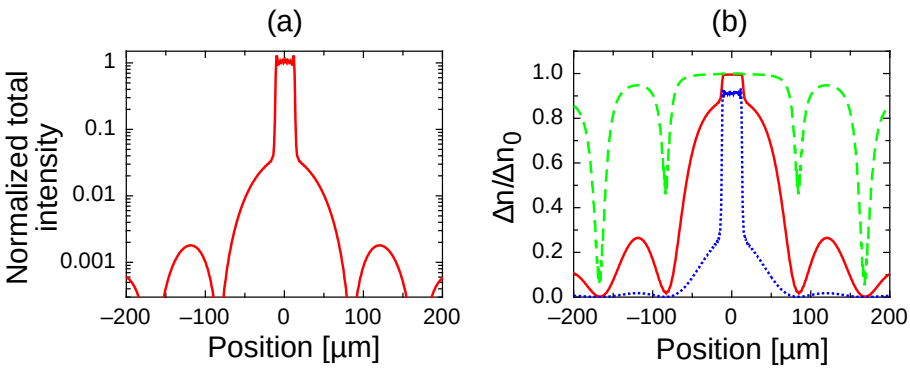

Fig. 5. (a) Light intensity $I = I_1 + I_2$ for the parameters $2a = 25\mu$m, $d_1 = 10\mu$m, $d_2 = 9.5$ mm, $n = 2.33$, $\alpha = 0.26$ cm^{-1}; (b) Refractive index distribution just after removal of the applied field for $I_D = 0.005$ (red solid curve), $I_D = 0.1$ (blue dotted curve), and $I_D = 0.0001$ (green dashed curve).

values of I_D (green dashed line in Fig. 5(b)), the formation of the central initial waveguide over the plateau is prevented and the probe light would no longer be guided before the removal of the applied field.

With the knowledge of the intensities $I_1(x)$ and $I_2(x)$ and of the initial distribution $\Delta n(x, t = 0)$, we can calculate the evolution of the refractive index profile of the waveguide using Eq. (2). This z-independent profile can then be used to calculate the propagation of the red probe wave at any time by the beam propagation method [13, 14]. As an example, Fig. 6 shows the calculated dynamics for SBN upon removal of the applied field. The temporal evolution of the probe beam propagation is calculated for a set of parameters corresponding to those used experimentally. The maximum refractive index change $\Delta n_0 = 3.5 \times 10^{-4}$ used in the simulation can be induced by a field $E_0 = 2.4$ kV/cm (corresponding to the intermediate field in Fig. 3) via the electro-optic coefficient $r_{333} = 235$ pm/V of SBN (x = 0.61) [20].

Figure 6 shows the temporal evolution of the probe wave propagation, of the refractive index profile and of the probe wave output intensity. At the time $t = 0$ the refractive index profile corresponds to the one given by the solid line in Fig. 5(b), the index contrast between the central region and the plateau is enough to guide the probe wave, in agreement with the experiments. The following simulated time evolution shows that the probe light is rapidly expelled from the initial central waveguide, it reaches the maximum distance for a time of the order of 5 times the photorefractive response time τ_{PR}, before slowly relaxing back to a straight propagation. The calculated dynamics of the waveguide splitting process is in good qualitative agreement with the observed one (see Fig. 2 and Fig. 3). The simulated spot separation distances are consistent with those observed experimentally. We recall that the simulations are calculated under simplified ideal conditions. The strong effect of the border of the refractive index change profile associated to the central lobe of the diffracting back reflected control light is a consequence of this simplication. In the experimental situation, any scattering stray light, as well as multiple reflections, contribute to smooth the refractive index contrast at the border of the central lobe.

Our observations of Fig. 3 show that the probe light splits faster and further apart if the field that is applied during the primary waveguide recording is larger. Figure 7 shows a snapshot of the initial splitting ($t = 0.3$) of the probe wave for three values of Δn_0 corresponding to the three values of the field in Fig. 3. The stronger initial spatial splitting for the higher fields can be easily recognized, in agreement with the experimental observations. It has to be noted, that for materials with short diffusion lengths, such as our SBN crystal, the photorefractive response

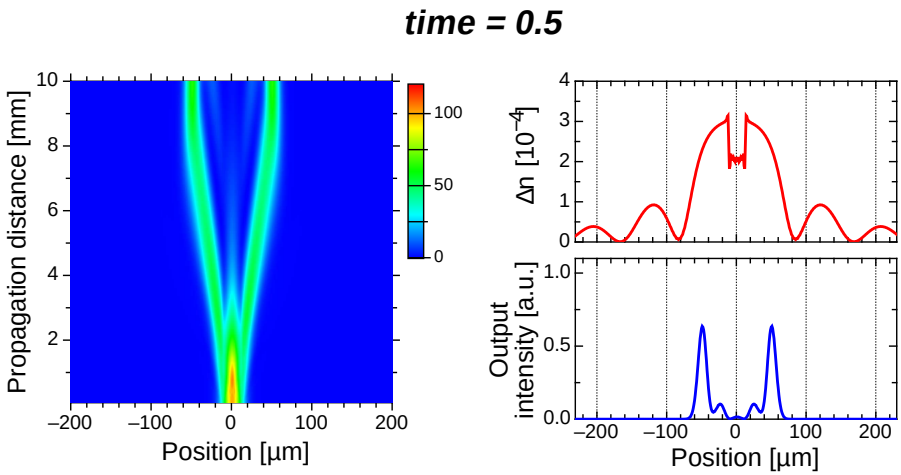

Fig. 6. (1.5 MB) Simulated time evolution of the waveguide splitting phenomenon after removing the sustaining applied electric field at the time $t = 0$. The left-hand side shows the propagation of the probe beam in the SBN crystal containing the splitted photoinduced waveguide with the given color scale for its intensity. The top-right diagram shows the evolution of the refractive index profile according to Eq. (2). The bottom-right diagram shows the profile of the probe beam intensity on the output surface of the crystal. Parameters: $\Delta n_0 = 3.5 \times 10^{-4}$, $I_D = 0.005$, input waist of probe beam = 18 μm. All other parameters as in Fig. 5. The time is normalized to the photorefractive response time. The temporal distance between frames is not constant.

time is a decreasing function of the electric field [18]. Therefore, the same normalized time corresponds to an earlier "real" time for the case of a large field than for the case of a low field. This effect contributes to accelerate further the dynamics for the larger fields with respect to what appears from Fig. 7.

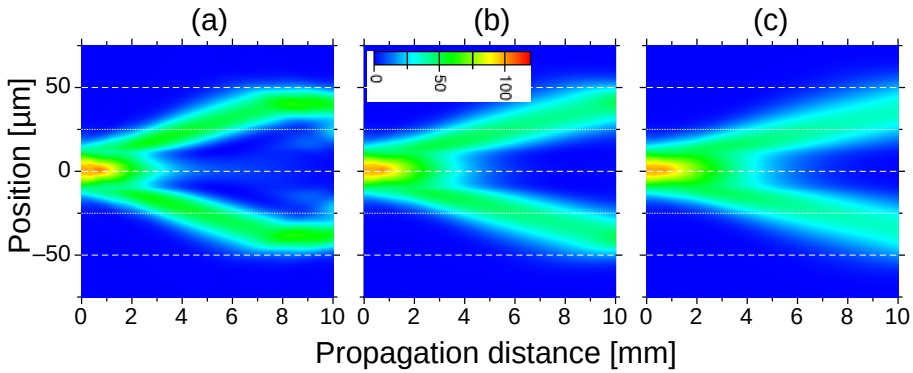

Fig. 7. Initial splitting of the waveguide at the normalized time $t = 0.3$ for three values of Δn_0. (a) $\Delta n_0 = 6 \times 10^{-4}$ ($E_0 \approx$4 kV/cm); (b) $\Delta n_0 = 3.5 \times 10^{-4}$ ($E_0 \approx$2.4 kV/cm); $\Delta n_0 = 2.4 \times 10^{-4}$ ($E_0 \approx$1.6 kV/cm). The other parameters are as in Fig. 6.

4.2. $LiTaO_3$

In the case of $LiTaO_3$ the control light is strongly absorbed and induces direct band-to-band phototransitions. For such interband processes the quadratic recombination of carriers leads to

a photoconductivity which increases only with the square root of the light intensity [21]. This has an effect on the screening of the applied electric field. By assuming that the square root dependence is valid over the whole range of relevant intensities, Eqs. (1) and (2) have to be modified, and Eq. (2) is replaced by

$$\Delta n(x,t) = \Delta n_0 \frac{\sqrt{I(x)}}{\sqrt{I(x)}+\sqrt{I_D}} \exp\left[-t\left(\sqrt{I(x)}+\sqrt{I_D}\right)\right]. \tag{5}$$

Here the same intensity normalization as above is used and the role of I_D is the same as in the case of SBN. Due to the large absorption constant (≈ 690 cm^{-1} [12]), the back reflected control wave $I_2(x)$ does not play any role in the case of $LiTaO_3$. Nevertheless, in the absence of a background illumination a significant widening of the primary waveguide during recording (with field on) is observed, as was discussed in [2]. This widening is due to control light surrounding the ideal imaged slit defining the waveguide (stray light). A combination of diffraction effects (described in first approximation by the function $I_1(x)$ of Eq. (3)) and of scattering effects due to bulk defects or surface imperfections (more difficult to describe mathematically) is expected to contribute to the stray light producing the widening. Even though the intensity level of the scattering might be very small, it can lead to quite strong widening because of the very low levels of the dark intensity I_D proper of $LiTaO_3$ under UV illumination. The quantity I_D can be estimated by considering the depth until which a holographic grating can be recorded by the UV light. This depth corresponds roughly to the position where $I/I_D = 1$ and is of the order of 250 μm [2] for crystals similar to the one used in our measurements. Using the above absorption constant we can then estimate a ratio of the order of $I/I_D = 10^5$ at the depth of 80-90 μm of our waveguides. The main reason for the very small value of I_D is the high quantum efficiency connected with the interband phototransitions. Below, we will discuss some simulations of the probe beam propagation in $LiTaO_3$ by considering the refractive index evolution given by Eq. (5). For simplicity we neglect the effect of scattering and limit the description of the stray light to the diffractive component by using the expression (3) for the control light intensity, always with a non vanishing value for the distance d_1.

Figure 8(a) shows the calculated propagation of the probe wave in the stationary state just before the applied field is removed. By considering the electro-optic response of $LiTaO_3$ [22], the refractive index amplitude Δn_0 used for the simulations corresponds to an applied field of 5.5 kV/cm. The wave is only badly guided due to the fact that the waveguide has suffered a significant widening, as seen by the refractive index distribution in Fig. 8(c), which applies to the same situation. Fig. 8(b) shows the same propagation but for a normalized time $t = 5$ after removing the applied electric field, which corresponds roughly to the moment of maximum separation. Figure 8(d) shows the refractive index distribution at the same time. As in the case of SBN, we observe the splitting of the propagating wave into two lobes. However, the calculated separation distance between the lobes is smaller than in SBN, which is in agreement with the observations in the two crystals (compare Fig. 2 and Fig. 4) and with the model simulations for SBN (Fig. 6).

As discussed earlier, the near field experimental observations in $LiTaO_3$ (Fig. 4) show that the two lobes are slightly tilted with a larger separation closer to the entrance surface of the control light. Due to the large absorption, a change in depth is connected to a change of the normalized dark intensity I_D. We discuss the lobe tilt with the help of Fig. 8(e), where we have calculated the output intensity profile of the probe beam for three different values of I_D, corresponding to three depths mutually separated by 35 μm. Together with I_D, we have changed also the value of the imaging mismatch d_1, increasing it from 10 μm for the top diagram in Fig. 8(e), to 45 μm for the middle one, and to 80 μm for the bottom one. In general, larger values of d_1 lead to wider intensity distributions that may lead to bigger spot separations. How-

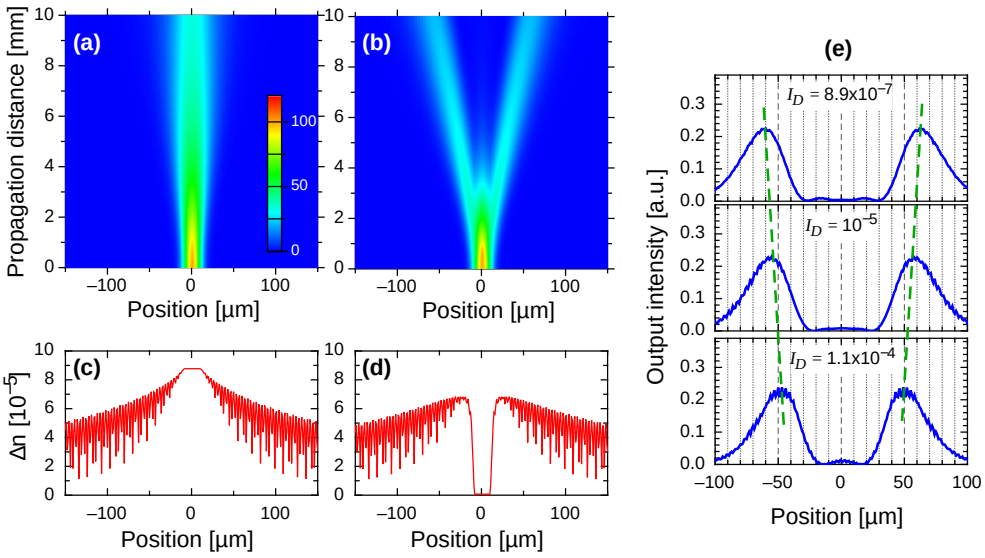

Fig. 8. Model calculations for the case of $LiTaO_3$ using Eqs. (3) and (5) with the parameters $\Delta n_0 = 8.8 \times 10^{-5}$, $2a = 20\mu$m, $n = 2.72$ and a probe beam input waist of 15 μm. (a) Probe beam propagation in the primary waveguide widened to steady-state at $t = 0$ for $I_D = 10^{-5}$ and $d_1 = 45$ μm. (b) Same as (a) but for the time $t = 5$ after splitting of the waveguide. (c) and (d) Refractive index profiles for case (a) and (b), respectively. (e) Output probe beam intensity profile at three depths for $t = 5$. The central diagram corresponds to the case (b). The upper diagram to a position 35 μm closer to the surface ($I_D = 8.9 \times 10^{-7}$, $d_1 = 10$ μm). The lower diagram to a position 35 μm deeper ($I_D = 1.1 \times 10^{-4}$, $d_1 = 80$ μm). The dashed green line is a guide for the eye evidencing the relation with the spot obliquity of Fig. 4.

ever, our simulations have shown that, for the range of intensity-to-dark-intensity ratio in which we operate experimentally, the change of the parameter d_1 has only a very small influence on the spot obliquity with respect to the influence of the normalized I_D. Indeed the simulations of Fig. 8(e) correctly predict a larger spot separation for the top diagram (see dashed green helping line) that corresponds to the layer closer to the surface. This larger separation is due to the stronger widening occurring for the larger values of the ratio I/I_D. The calculations predict a decrease of the separation by about 25-30 μm for a depth increase of 70 μm, which is in quite good agreement with the observations of Fig. 4, the absolute value of the spot separation is matched within roughly 20% between experiments and simulations. It is worth noticing that, if we perform the simulations using Eq. (2) instead as with Eq. (5), we obtain a much stronger dependence of the spot separation on the normalized value of I_D. The spot obliquity predicted by Eq. (2) is nearly doubled, what prevents to match the experimental data. This proves the necessity to take into account the square root dependence of the photoconductivity on the light intensity in the model.

5. Modulation of the transmitted light by waveguide anti-waveguide alternation

Since the removal of the electric field prevents the probe light to remain guided in its original photo-induced waveguide, we can use this effect for a novel light modulation technique. The application of a periodic high-voltage to the crystal leads to a waveguide and an anti-waveguide appearing cyclically at the place illuminated by the shaped control light. The modulation occurs through the coupling of the spatial position of the output beam to the electric field, without

changing any of the illumination conditions. Figure 9 shows an example of this modulation as obtained in SBN under a periodic applied field of triangular shape. Note that in the experiment of Fig. 9 we have deliberately slightly misaligned the incidence direction of the probe wave with respect to the axis of the waveguide. In this way, upon removal of the field, the light is expelled only on one side of the waveguide. In the example given in Fig. 9 , when considering the conditions separated by half a voltage cycle, the output position of the probe beam shifts by roughly 90 μm. When repeating the same kind of experiments with $LiTaO_3$ similar results are obtained, however the observed shift is of the order of 40 μm in this case.

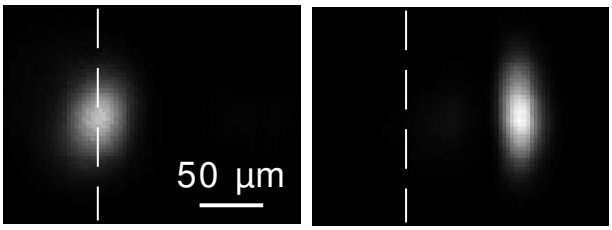

Fig. 9. (1.2 MB) Modulation of the output position of the probe beam under a periodic electric field. A triangularly shaped electric field with amplitude 2 kV/cm and frequency 1 Hz is applied to the crystals. The resulting waveguide-antiwaveguide alternation results in the periodically varying output position of the probe wave. The two frames shown above are separated by half a period, the corresponding displacement between the two positions is about 90 μm. SBN crystal, controlling wave intensity = 0.4 W/cm^2. The width of the imaged area in the multimedia file is 480 μm.

In order to better characterize the dynamics of the effect, we have inserted a small pinhole in the image plane of the crystal's output surface and detected the transmission through this pinhole by a photodiode. Figure 10 shows an example of this time dependence for the case of $LiTaO_3$ and three different frequencies of the applied field. The diameter of the measuring pinhole was one half the nominal width of the photoinduced waveguide. The intensity of the incident UV controlling light at the surface of the crystal was 1.1 W/cm^2. Considering that the waveguide was probed at an average depth of $\approx 90\mu$m, the local UV intensity in the probed region was ≈ 2 mW/cm^2. The dynamics of Fig. 10 is following the particular form of the voltage delivered by the high voltage power supply being used. Nevertheless, at the two higher frequencies, a slight delay between the maximum of the applied voltage and the maximum of the transmitted intensity can be recognized. In these conditions, the field can lead to an increase of the waveguide strength even at the beginning of its decreasing half period. When compared to the period T of the applied field, at the above intensity the resulting retardation between the red and blue curve is roughly $0.15 \times T$ for $T = 100$ ms, $0.04 \times T$ for $T = 335$ ms, while it becomes nearly irrelevant at lower frequencies. As can be expected due to a slower dynamics, this retardation increases if the controlling light intensity is reduced. For instance, for a 40 times lower intensity we get a phase retardation of $0.35 \times T$ at $T = 100$ ms. The maximum modulation amplitude of the transmitted probe light is found for the above experimental conditions in $LiTaO_3$ when the applied field period is in the range of 200–350 ms.

For similar experiments performed using SBN we obtain essentially the same kind of results as those depicted in Fig. 10. Here the optimum modulation amplitude is found for an applied electric field period of the order of 1 second (incident controlling light intensity = 90 mW/cm^2). At this intensity the retardation discussed above goes from $0.2 \times T$ at $T = 400$ ms down to $0.002 \times T$ at $T = 10$ s. It should be noted that in SBN, due to the much lower absorption of the controlling light, the observed dynamics is much less dependent on the probing depth below

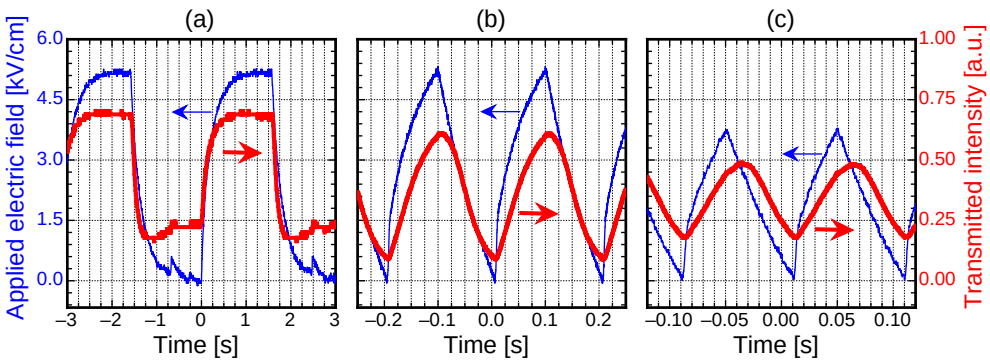

Fig. 10. Waveguide modulation dynamics for $LiTaO_3$ as measured by transmission of the probe wave through a pinhole (red thick line). The modulated applied field is shown by the thin blue line. a) 0.3 Hz modulation, b) 5 Hz, c) 10 Hz.

the surface as in the case of $LiTaO_3$.

6. Conclusions

The evolution of light induced one-dimensional waveguides when the sustaining electric field is switched off leads to a novel kind of dynamic light deflection. We have studied this effect in detail using SBN and $LiTaO_3$ crystals. Simulations of the beam propagation in the split waveguide on the base of a simple model lead to a good agreement with the experimental observations. In the case of SBN the spot separation can exceed the original waveguide width by 10 times. It is found that the control light back reflected from the second lateral surface is responsible for the additional waveguide widening, which leads to this large deflection distance. In $LiTaO_3$ the primary waveguide widening is due solely to stray light and gives smaller deflection distances. In this material the strong absorption constant leads to oblique spots after waveguide splitting which have been successfully modeled. Application of a modulated electric field leads to the modulation of the transmitted probe light as a result of a waveguide anti-waveguide alternation. This novel modulation method has been demonstrated for low frequencies of the applied field. Faster speeds are expected by increasing the local intensity of the controlling light. The use of materials with higher photosensitivity, such as $Sn_2P_2S_6$ or reduced $KNbO_3$, is also expected to lead to faster modulation speeds in a regime that uses the conventional photorefractive effect, which allows to obtain a waveguide dynamics being virtually independent from the observation depth.

Acknowledgements

This work was performed in the framework of the PAI bilateral program *Germaine de Staël* between France and Switzerland. We are very grateful to Dr. K. Kitamura (NIMS, Tsukuba, Japan) for the $LiTaO_3$ crystals. F. J., M. J. and P. G. also acknowledge partial support by the Swiss National Science Foundation.